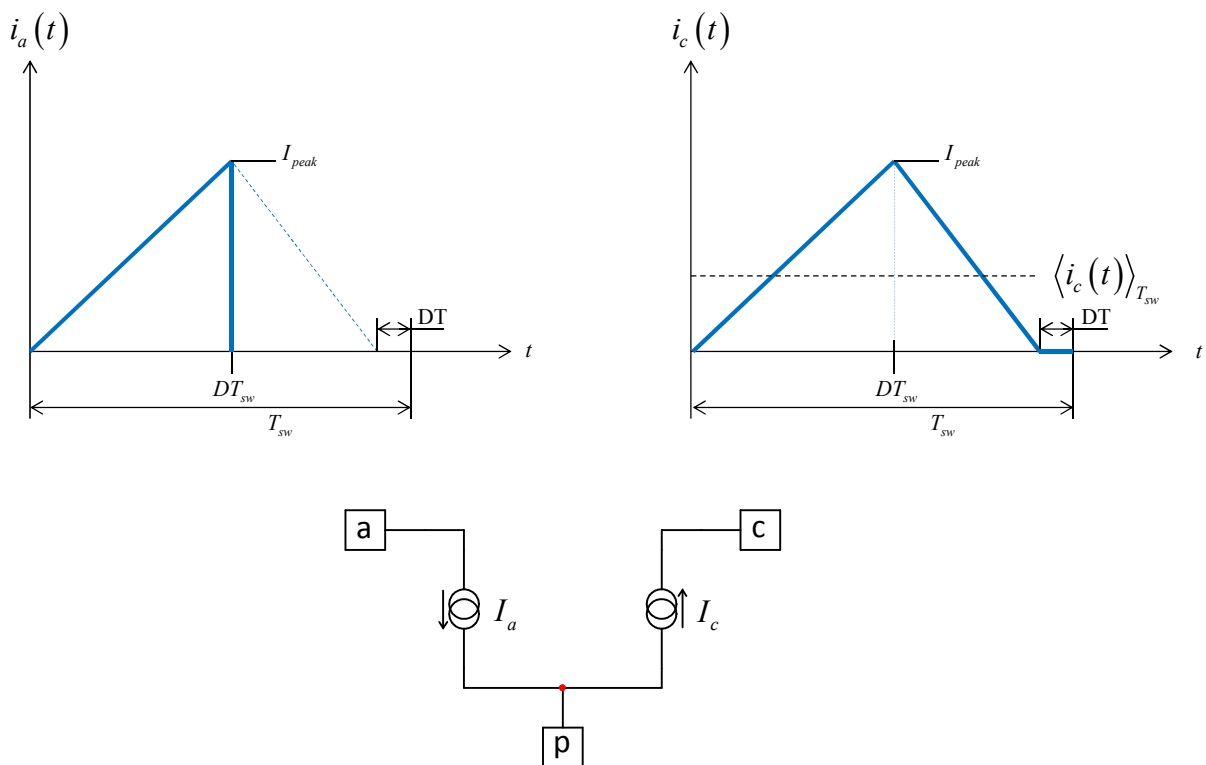


# A Small-Signal Model of the Flyback Converter Operated in QR Including Dead Time for Multiple Valley Switching

Christophe Basso

In Chap. 2 of [1], we have introduced a large-signal model of the PWM switch operated in the so-called quasi-square wave resonant mode, also known as quasi resonant (QR) or borderline conduction mode (BCM). When calculating the model operational parameters, we considered the re-start of the power switch exactly where the inductor current reaches zero. In reality, the designer always introduces a small dead time (DT) to make sure the power switch is reactivated exactly at the minimum of the drain-source wave. This is to reduce or even cancel turn-on losses by reflecting enough voltage at turn-off. Furthermore, in light-load conditions, modern controllers fold the switching frequency back to improve the efficiency. This is done by expanding the dead time and jumping in the valley 2, 3, 4 and so on. How do dead time and multiple valley jump affect the transfer function, this is the object of this analysis.

In order to analytically obtain the control-to-output transfer function of a current-mode flyback converter operated in the QR mode with multiple valley switching, a small-signal model has to be derived. In a converter operated in BCM with dead time, the average current flowing through terminal “c” is no longer the peak current value divided by 2. Typical waveforms from the BCM PWM switch model appears in Figure 1. They are actually waveforms of the PWM switch model operated in discontinuous conduction mode whose switching period is affected by the self-relaxing nature of the QR scheme.



**Figure 1:** the PWM switch model in Borderline Conduction Mode once simplified.

The dead time  $DT$  is a delay inserted when core reset has been detected to make sure the power switch is turned on right in the minimum of the drain-source valley. From the starting point of the sinusoidal waveform, it corresponds to half of the period:

$$DT = \pi \sqrt{L_p C_{lump}} \quad (1)$$

Generalized over valley 2, 3 etc, (1) becomes:

$$DT = (2n-1) \pi \sqrt{L_p C_{lump}} \quad (2)$$

In which  $n$  is the valley number. In this model, we have the following source definitions already derived in Chap. 2 of [1]:

$$d_1 = \frac{V_c}{R_i} \frac{L}{V_{ac} T_{sw}} \quad (3)$$

$$t_{on} = \frac{V_c}{R_i} \frac{L}{V_{ac}} \quad (4)$$

$$d_2 = \frac{V_c}{R_i} \frac{L}{V_{cp} T_{sw}} \quad (5)$$

$$t_{off} = \frac{V_c}{R_i} \frac{L}{V_{cp}} \quad (6)$$

The switching period is then the sum of  $t_{on}$  and  $t_{off}$  plus the dead time.

$$T_{sw} = \frac{V_c L}{R_i} \left( \frac{1}{V_{ac}} + \frac{1}{V_{cp}} \right) + DT \quad (7)$$

The average current in terminal c is no longer  $I_{peak}/2$  as with the previous QR model. It becomes a function of  $d_1$  and  $d_2$ :

$$I_c = \frac{V_c}{R_i} \left( \frac{d_1 + d_2}{2} \right) = \left( \frac{V_c}{R_i} \right)^2 \frac{L(V_{ac} + V_{cp})}{2T_{sw} V_{ac} V_{cp}} \quad (8)$$

If we substitute (3), (5) and (7) in (8) and rearranging we have:

$$I_c = \frac{V_c}{2R_i} \frac{V_{ac} + V_{cp}}{V_{ac} + V_{cp} + \frac{DT \cdot R_i V_{ac} V_{cp}}{LV_c}} \quad (9)$$

Please note that this equation simplifies to  $I_c = V_c/2R_i$  which is the  $I_c$  definition of the original QR model for a null dead time ( $DT = 0$  in (9)).

In the primary side, the  $I_a$  source is no longer  $DI_c$  as with the QR model. It should be replaced by the  $I_a$  generator already developed for the DCM model in Chapter 2:

$$I_a = \frac{I_{peak}}{2} d_1 = I_c \frac{d_1}{d_1 + d_2} \quad (10)$$

If we use (3) and (5) to substitute them in (10), we have:

$$I_a = I_c \frac{V_{cp}}{V_{ac} + V_{cp}} \quad (11)$$

Further rearranging using (9), we have:

$$I_a = \frac{V_c}{2R_i \left( \frac{V_{ac}}{V_{cp}} + 1 + DT \frac{R_i}{L} \frac{V_{ac}}{V_c} \right)} \quad (12)$$

Classical small-signal analysis requires the linearization of the above large-signal sources,  $I_a$  and  $I_c$ . We can automate this calculation using partial differentiation:

$$\hat{i}_c = \frac{\partial I_c(V_c, V_{ac}, V_{cp})}{\partial V_c} \hat{v}_c + \frac{\partial I_c(V_c, V_{ac}, V_{cp})}{\partial V_{ac}} \hat{v}_{ac} + \frac{\partial I_c(V_c, V_{ac}, V_{cp})}{\partial V_{cp}} \hat{v}_{cp} \quad (13)$$

and put it under the form:

$$\hat{i}_c = k_1 \hat{v}_c + k_2 \hat{v}_{ac} + k_3 \hat{v}_{cp} \quad (14)$$

in which

$$k_1 = \frac{L_p V_c (V_{ac} + V_{cp}) (L_p V_c V_{ac} + L_p V_c V_{cp} + 2 \cdot DT \cdot R_i V_{ac} V_{cp})}{2R_i (L_p V_c V_{ac} + L_p V_c V_{cp} + DT \cdot R_i V_{ac} V_{cp})^2} \quad (15)$$

$$k_2 = -\frac{DT \cdot L_p V_c^2 V_{cp}^2}{2(L_p V_c V_{ac} + L_p V_c V_{cp} + DT \cdot R_i V_{ac} V_{cp})^2} \quad (16)$$

$$k_3 = -\frac{DT \cdot L_p V_c^2 V_{ac}^2}{2(L_p V_c V_{ac} + L_p V_c V_{cp} + DT \cdot R_i V_{ac} V_{cp})^2} \quad (17)$$

For the  $I_a$  current, we have:

$$\hat{i}_a = \frac{\partial I_a(V_c, V_{ac}, V_{cp})}{\partial V_c} \hat{v}_c + \frac{\partial I_a(V_c, V_{ac}, V_{cp})}{\partial V_{ac}} \hat{v}_{ac} + \frac{\partial I_a(V_c, V_{ac}, V_{cp})}{\partial V_{cp}} \hat{v}_{cp} \quad (18)$$

which can put under the form:

$$\hat{i}_a = k_4 \hat{v}_c + k_5 \hat{v}_{ac} + k_6 \hat{v}_{cp} \quad (19)$$

where

$$k_4 = \frac{L_p V_c V_{cp} (L_p V_c V_{ac} + L_p V_c V_{cp} + 2 \cdot DT \cdot R_i V_{ac} V_{cp})}{2 R_i (L_p V_c V_{ac} + L_p V_c V_{cp} + DT \cdot R_i V_{ac} V_{cp})^2} \quad (20)$$

$$k_5 = - \frac{V_c \left( \frac{1}{V_{cp}} + \frac{DT \cdot R_i}{L_p V_c} \right)}{2 R_i \left( \frac{V_{ac}}{V_{cp}} + \frac{DT \cdot R_i V_{ac}}{L_p V_c} + 1 \right)^2} \quad (21)$$

$$k_6 = \frac{V_c V_{ac}}{2 R_i V_{cp}^2 \left( \frac{V_{ac}}{V_{cp}} + \frac{DT \cdot R_i V_{ac}}{L_p V_c} + 1 \right)^2} \quad (22)$$

Re-arranging the original large-signal model with these new source definitions, the updated small-signal model appears in Figure 2:

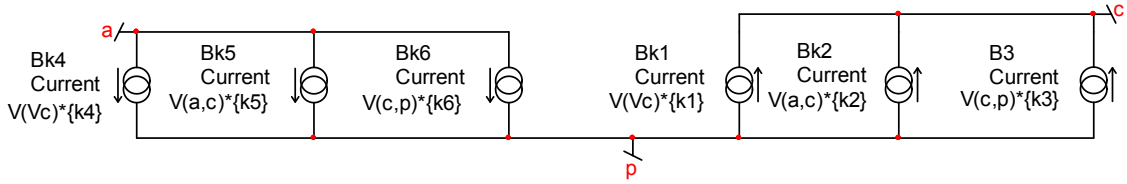


**Figure 2:** the updated small-signal model uses 5 current sources and an equivalent resistor  $R_7$ .

### A BCM Flyback Converter

Our main application is a flyback converter operated in peak current-mode control Borderline Conduction Mode. The implementation of the BCM small-signal model in this configuration appears in Figure 3. It is the PWM switch model rotated to fit the buck-boost configuration to which we have added the isolation transformer. The left panel automates the various coefficients calculations. In the flyback configuration, we have the following voltage correspondence:

$$V_{ac} = V_{in} \quad (23)$$

$$V_{cp} = \frac{V_{out}}{N} \quad (24)$$

If we assume the following component values:

$$V_{in} = 100 \text{ V}$$

$$L_p = 450 \mu\text{H}$$

$$R_i = 250 \text{ m}\Omega$$

$$P_{out} = 70 \text{ W}$$

$$V_{out} = 19 \text{ V}$$

$$R_{load} = 2.057 \Omega$$

$$C_{lump} = 200 \text{ pF}$$

$$r_C = 50 \text{ m}\Omega$$

$$C_{out} = 1.5 \text{ mF}$$

$$n = 6$$

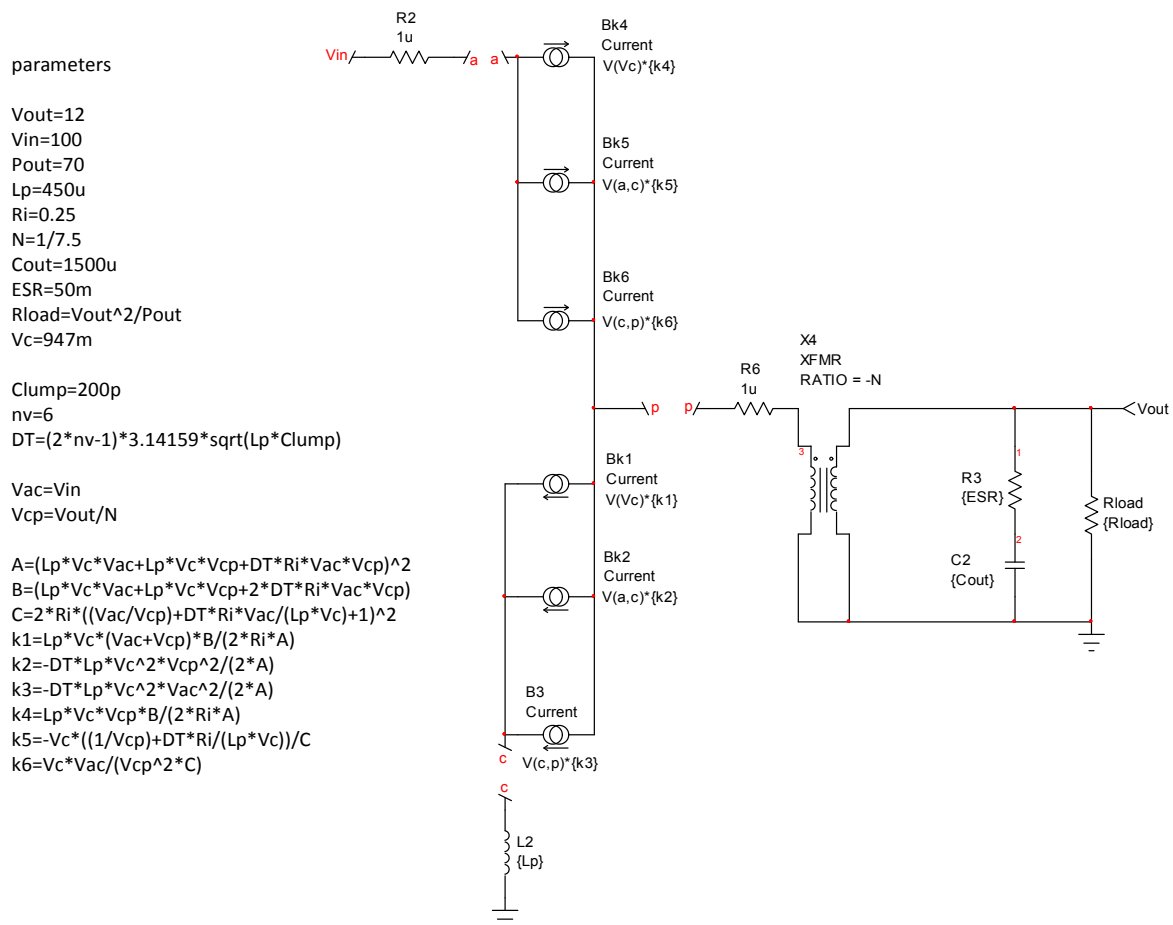


**Figure 3:** the small-signal model with a flyback converter. Coefficients are automated in the left panel.

The large-signal PWM switch model in QR has been updated with the following code, to account for the dead time contribution:

```
.subckt PWMQR a c p vc ton fsw params : L=1.2m Ri=0.5 DT=1
*
* This subckt is a current-mode BCM model, version 1
*
```

```

.subckt limit d dc params: clampH=0.99 clampL=16m
*
Gd 0 dcx d 0 100u
Rdc dcx 0 10k
V1 clpn 0 {clampL}
V2 clpp 0 {clampH}
D1 clpn dcx dclamp
D2 dcx clpp dclamp
Bdc dc 0 V=V(dcx)
.model dclamp d n=0.01 rs=100m
.ENDS
*
Btsw tsw 0 V= ( (V(vc)*{L}/{Ri}) * ( 1/v(a,cx) + 1/v(cx,p) ) + {DT} ) *1Meg
Bdc dcx 0 V=V(vc)*{L}/{Ri}*V(a,cx)*(V(tsw)/1Meg)
Xdc dcx dc limit params: clampH=0.99 clampL=7m
BIap a p I=I(VM)*V(dc)/(V(dc)+V(d2))
Bd2 d2 0 V=V(vc)*{L}/{Ri}*V(c,p)*(V(tsw)/1Meg)
BIpc p cx I=V(vc)/{Ri}
BImju cx p I=(v(cx,p)/{L})*V(d2)*(V(tsw)/1Meg)*(1-(V(dc)+V(d2))/2)
Bton ton 0 V = V(dc)*v(tsw)
Bfsw fsw 0 V = (1/(V(tsw)/1Meg))/1k
Rdum1 vc 0 1Meg
VM cx c
*
.ENDS

```

If we compare the ac response given by the small-signal model and the large-signal QR PWM switch model, their responses are identical (Figure 4). This validates the first part of our small-signal analysis.

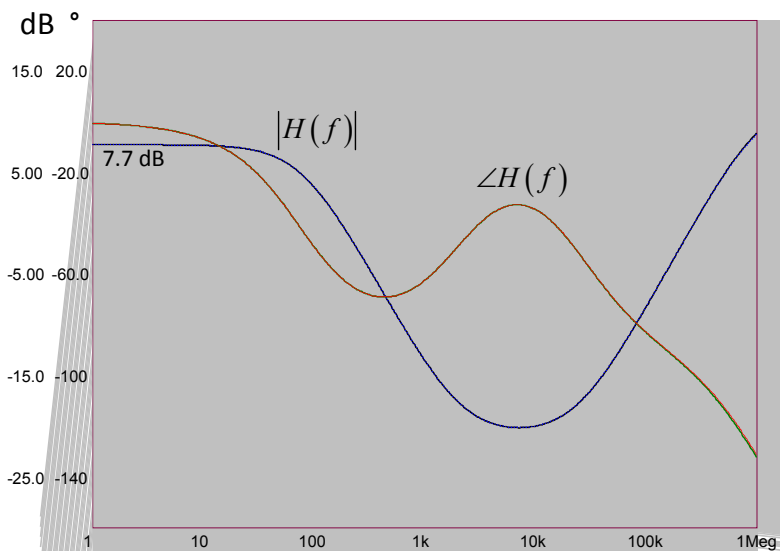


**Figure 4:** both models deliver a similar ac response which is encouraging to pursue the analysis. Here the response in valley 6.

Figure 3 schematic can now be recaptured considering the absence of ac contribution from the input voltage. Therefore, node “a” is ac-grounded, leading to a nice simplification. The new circuit appears in Figure 5.

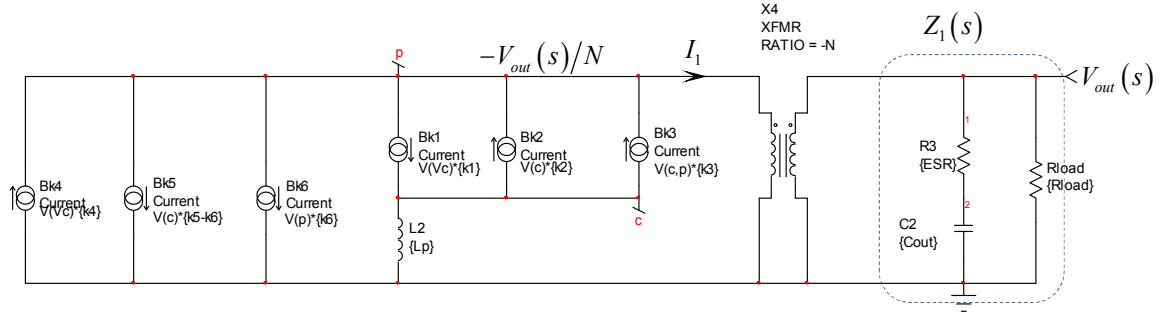


**Figure 5:** considering an ac-grounded input, sources featuring node “a” in their expression can be simplified.

### Deriving the Control-to-Output Transfer Function

We can use classical node/mesh analysis to start the analysis. The voltage at node (c) depends on the current leaving node (c) and crossing the inductor  $L_p$ :

$$V_{(c)}(s) = I_c(s) s L_p \quad (25)$$

The current leaving terminal (c) is driven by sources  $B_{k1}$ ,  $B_{k2}$  and  $B_{k3}$ . Please note that for  $B_{k3}$ , we have:

$$B_{k3} = V(c, p) k_3 = V_{(c)} k_3 - V_{(p)} k_3 = k_3 \left( V_{(c)} + \frac{V_{out}}{N} \right) \quad (26)$$

Hence

$$I_c(s) = V_c(s) k_1 - V_{(c)} k_2 + \left( V_{(c)} + \frac{V_{out}(s)}{N} \right) k_3 \quad (27)$$

From (25)  $V_{(c)}$  is extracted and substituted in (27). We obtain a definition for  $I_c$ :

$$I_c(s) = \frac{V_{out}(s) k_3 + N V_c(s) k_1}{N(1 + s L_p k_2 - s L_p k_3)} \quad (28)$$

The current  $I_1$  entering the transformer is equal to:

$$I_1(s) = V_c(s) k_4 - I_c(s) s L_p (k_5 - k_6) + \frac{V_{out}}{N} k_6 - I_c(s) \quad (29)$$

Substituting (28) in (29), we obtain a nice equation:

$$I_1(s) = - \frac{V_{out}(s)(k_3 - k_6) + N V_c(s)(k_1 - k_4) + s L_p V_{out}(s)(k_3 k_5 - k_2 k_6) + s V_c(s) N L_p (k_5 k_1 - k_2 k_4 - k_1 k_6 + k_3 k_4)}{N[1 + s L_p (k_2 - k_3)]}$$

(30)

The output voltage is actually the current  $I_1(s)$  flowing into the output complex impedance  $Z_1(s)$  and scaled by the turns ratio  $-N$ :

$$V_{out}(s) = -NZ_1(s)I_1(s) \quad (31)$$

The impedance  $Z_1$  is made of a series-parallel arrangement of the output capacitor and its ESR plus the load resistance:

$$Z_1(s) = \frac{\left(\frac{r_c}{N^2} + \frac{1}{sC_{out}N^2}\right) \frac{R_{load}}{N^2}}{\left(\frac{r_c}{N^2} + \frac{1}{sC_{out}N^2}\right) + \frac{R_{load}}{N^2}} = \frac{R_{load}}{N^2} \frac{1 + sr_c C_{out}}{1 + sC_{out}(R_{load} + r_c)} \quad (32)$$

The control voltage delivered by the error amplifier is divided in the control circuit. This is the coefficient  $Div$ , equal to 4 in our case. If you substitute (30) and (32) into (31), then after a good glass of wine, you obtain the following transfer function:

$$H(s) = \frac{V_{out}(s)}{V_c(s)} = \frac{NR_{load}}{Div \cdot [N^2 + R_{load}(k_6 - k_3)]} \frac{(1 + sr_c C_{out})(k_1 - k_4 + sL_p(k_1k_5 - k_2k_4 - k_1k_6 + k_3k_4))}{1 + a_1s + a_2s^2} \quad (33)$$

Where the raw definitions for  $a_1$  and  $a_2$  are

$$a_1 = \frac{C_{out}N^2R_{load} + C_{out}N^2r_c + L_pN^2k_2 - L_pN^2k_3 - C_{out}R_{load}k_3r_c + C_{out}R_{load}k_6r_c - L_pR_{load}k_2k_6 - L_pR_{load}k_3k_5}{N^2 + R_{load}(k_6 - k_3)} \quad (34)$$

$$a_2 = \frac{Div \cdot C_{out}L_p(N^2R_{load}k_3 - N^2R_{load}k_2 - N^2k_2r_c + N^2k_3r_c + R_{load}r_c k_2k_6 + R_{load}r_c k_3k_5)}{Div \cdot [R_{load}(k_3 - k_6) - N^2]} \quad (35)$$

Rearranging and factoring (33), we obtain the final transfer function we are looking for:

$$H(s) = \frac{NR_{load}(k_1 - k_4)}{Div \cdot [N^2 + R_{load}(k_6 - k_3)]} \frac{(1 + sr_c C_{out}) \left(1 + sL_p \frac{k_1k_5 - k_2k_4 - k_1k_6 + k_3k_4}{k_1 - k_4}\right)}{1 + a_1s + a_2s^2} \quad (36)$$

The quality factor  $Q$  is equal to



$$Q = \frac{\sqrt{a_2}}{a_1} \quad (37)$$

While the resonant frequency is

$$\omega_0 = \frac{1}{\sqrt{a_2}} \quad (38)$$

Calculations show that  $Q$  is extremely low, we can thus apply the low- $Q$  approximation:

$$1 + \frac{s}{\omega_0 Q} + \left(\frac{s}{\omega_0}\right)^2 \approx \left(1 + \frac{s}{\omega_{p_1}}\right) \left(1 + \frac{s}{\omega_{p_2}}\right) \quad (39)$$

In which  $\omega_{p_1} = \omega_0 Q$  and  $\omega_{p_2} = \frac{\omega_0}{Q}$ . If we replace  $\omega_0$  and  $Q$  by their respective definitions, we have:

$$\omega_{p_1} = \frac{N^2 + R_{load}(k_6 - k_3)}{C_{out}N^2(R_{load} + r_C) + L_p N^2(k_2 - k_3) - C_{out}R_{load}r_C(k_6 - k_3) - L_p R_{load}(k_2 k_6 + k_3 k_5)} \quad (40)$$

$L_p$  and  $r_C$  are much smaller than 1, therefore, the above equation simplifies to:

$$\omega_{p_1} \approx \frac{1}{C_{out} \frac{R_{load} + r_C}{1 + \frac{R_{load}(k_6 - k_3)}{N^2}}} \quad (41)$$

The second pole is a high-frequency pole and can be neglected for crossover frequencies less than 10 kHz.

The LHP zero is a classical one

$$\omega_{z_1} = \frac{1}{r_C C_{out}} \quad (42)$$

While the second zero is a RHP type:

$$\omega_{z_2} = \frac{k_1 - k_4}{L_p(k_1 k_5 - k_2 k_4 - k_1 k_6 + k_3 k_4)} \quad (43)$$

Finally, the dc gain  $G_0$  can be expressed as:

$$G_0 = \frac{NR_{load}(k_1 - k_4)}{\text{Div} \cdot [N^2 + R_{load}(k_6 - k_3)]} \quad (44)$$

The final control-to-output transfer function of the QR converter featuring multiple valley switching is

$$H(s) \approx G_0 \frac{\left(1 + \frac{s}{\omega_{z_1}}\right) \left(1 + \frac{s}{\omega_{z_2}}\right)}{1 + \frac{s}{\omega_{p_1}}} \quad (45)$$

### Application example

A simple open-loop flyback has been assembled using the new large-signal PWM switch model in QR is proposed in Figure 6. It gives various operating points such as switching frequency and on time. The frequency can be computed the following way as shown in [1], where the parameter DT corresponds to the valley selection. It is 6 in our example.

$$F_{sw} = \frac{4}{\left( \sqrt{4DT + \frac{2L_p P_{out} (V_f + V_{out} + NV_{in})^2}{\eta V_{in}^2 (V_{out} + V_f)^2}} + \frac{\sqrt{2} L_p (V_f + V_{out} + NV_{in}) \sqrt{\frac{P_{out}}{\eta L_p}}}{V_{in} (V_{out} + V_f)} \right)^2} = 21.505 \text{ kHz} \quad (46)$$

The on time is calculated to 16.99  $\mu$ s. The peak current is 947 mA. These values are those calculated by the QR model for a 12-V output. A 100% efficiency is considered in this case ( $V_f = 0$ ).

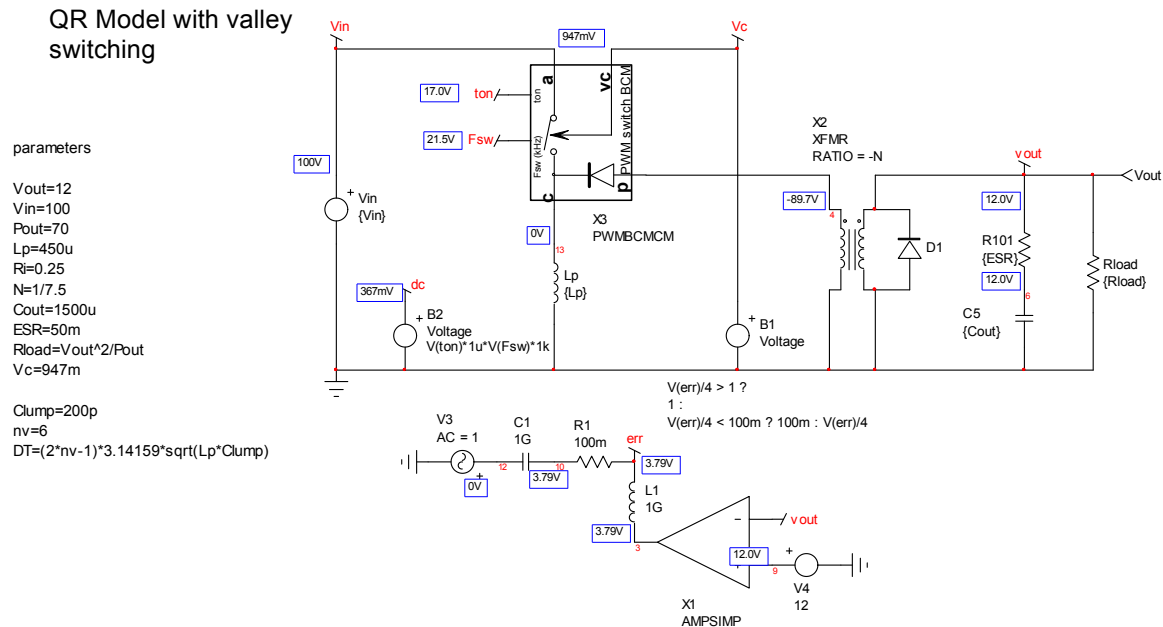


**Figure 6:** the large-signal QR PWM switch model will tell us if derivations of various parameters are ok.

The dominant low-frequency pole is calculated at around 79 Hz while the RHPZ is located at 24 kHz. The dc gain is found to be 7.7 dB. To check simulation versus our analytical results, we have superimposed the ac curve delivered by SPICE with that delivered by Mathcad®. The dc gain is exactly 7.7 dB as predicted and ac responses are perfectly matched.

Now, let's switch the valley number to 3. For the same amount of power, the frequency is now 27 kHz and the dc gain is calculated to 8.3 dB. Both responses (SPICE and Mathcad®) are shown in Figure 8.

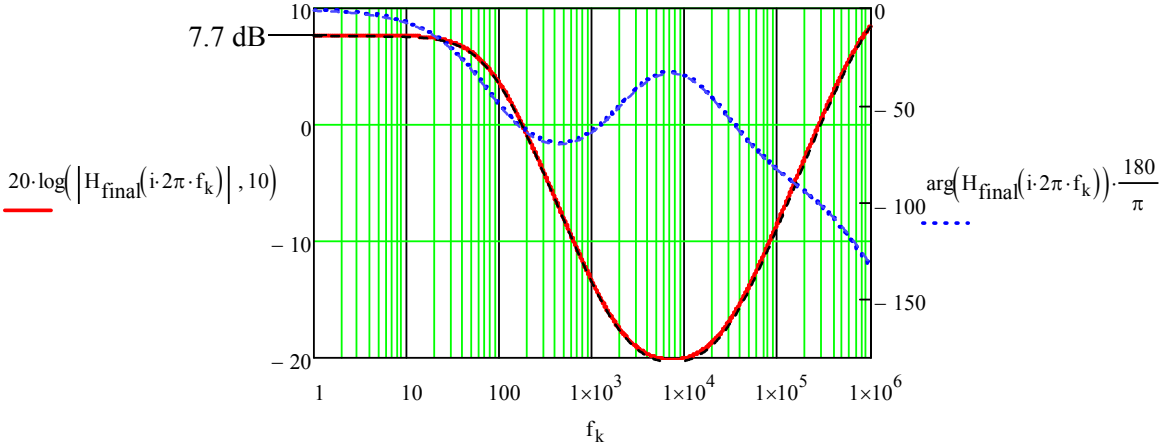


**Figure 7:** the response delivered by the SPICE model matches that calculated by Mathcad®. Valley number is 6.

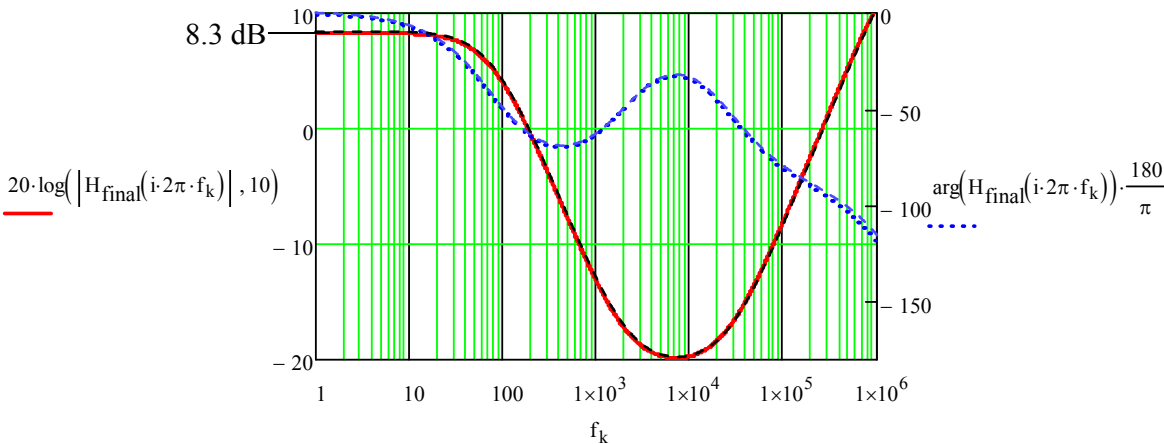
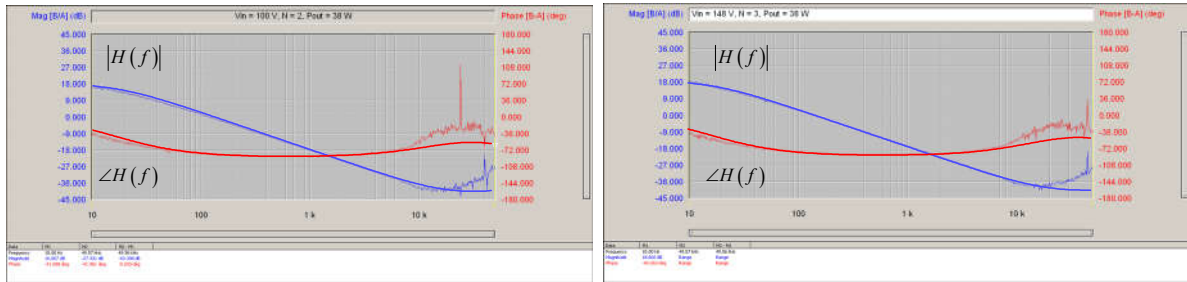


**Figure 8:** the response delivered by the SPICE model matches that calculated by Mathcad®. Valley number is 3.

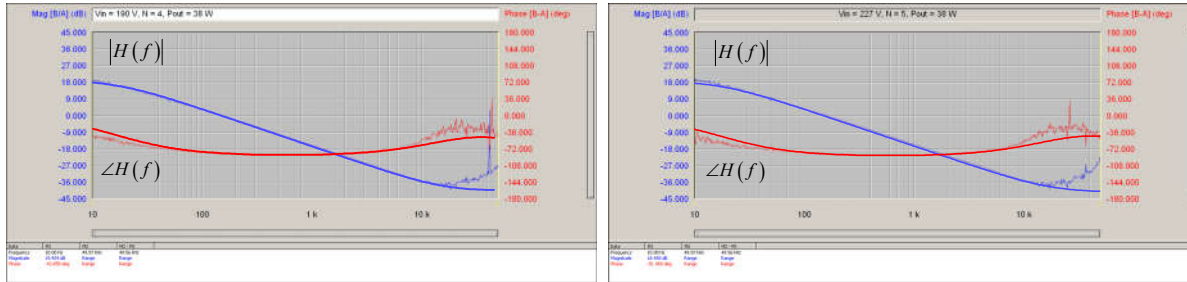
**Experiments on the Bench**

A QR board has been built around the NCP1339, a multiple valley controller recently released by ON Semiconductor. It is a 19-V/60-W universal mains ac-dc adapter. The controller allows a jump in valley 1 to 6 as the load is getting lighter. For the experiment, we have imposed a fixed load and we increased the input voltage to force operation in different valleys. Power stage ac response was then captured with an AP300 analyzer.



$V_{in} = 100 \text{ V}, N = 2 \quad G(10 \text{ Hz}) = 16.1 \text{ dB}$

$V_{in} = 148 \text{ V}, N = 3 \quad G(10 \text{ Hz}) = 18.6 \text{ dB}$



$V_{in} = 190 \text{ V}, N = 4 \quad G(10 \text{ Hz}) = 19.4 \text{ dB}$

$V_{in} = 227 \text{ V}, N = 5 \quad G(10 \text{ Hz}) = 18.5 \text{ dB}$

**Figure 9:** the various dynamic responses captured on the bench are in good agreement with the simulated results.

The results are gathered in Figure 9 and the agreement between the model and the bench measurements are quite good. Now that the model is validated, we can use the simulation schematic from Figure 6 and see the effect of varying the valley number on the overall response. As shown in Figure 10, the contribution of the valley number if it affects indeed the switching frequency and the peak current setpoint it has only a very small influence on the overall shape and can be neglected during loop analysis.

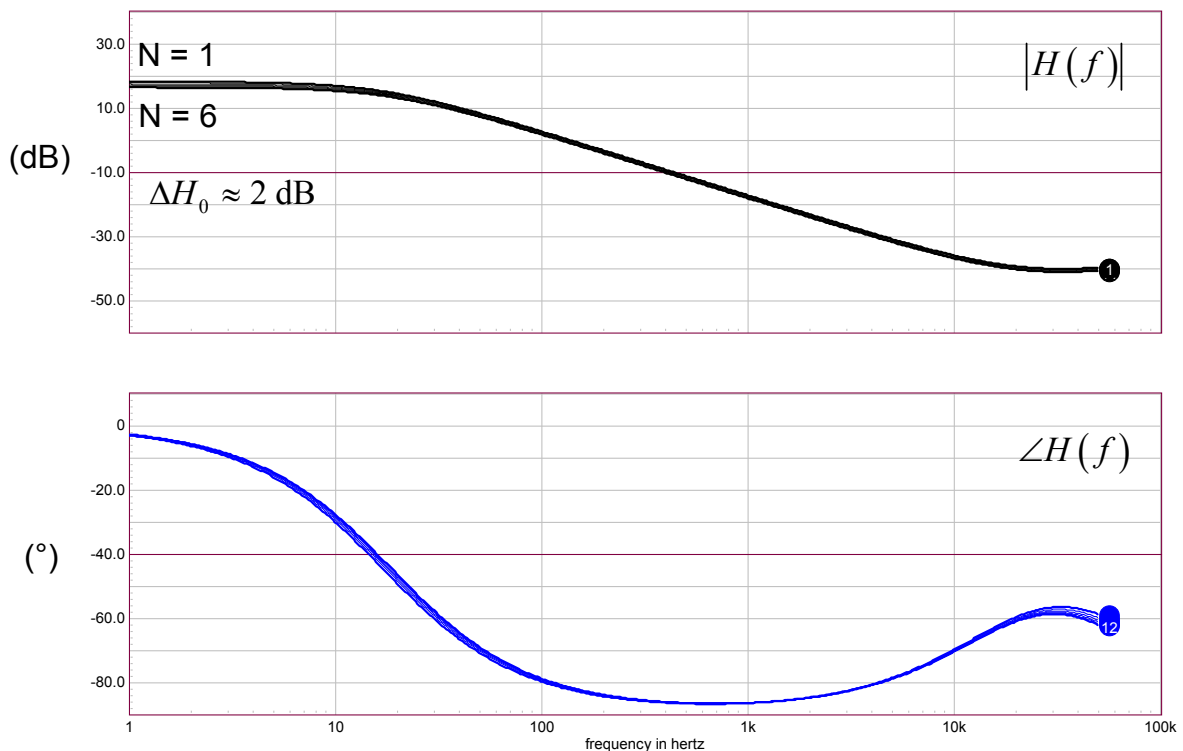


**Figure 10:** changing the valley from the first to the sixth brings a small static gain variation of less than 2 dB.

## **Conclusion**

This paper shows how the small-signal model of the BCM flyback converter operating in multiple valleys can be derived using the PWM switch model. Bench experiments confirm the calculations and show the negligible effect brought by the jump in different valleys. The action on the overall dynamic response can thus be neglected when studying the loop response.

---

## **References**

1. C. Basso, "Switch Mode Power Supplies: SPICE Simulations and Practical Designs – second edition", McGraw-Hill 2014